Endocytosis of Wingless via a dynamin-independent pathway is necessary for signaling in *Drosophila* wing discs

Anupama Hemalatha[a], Chaitra Prabhakara[a], and Satyajit Mayor[a,b,1]

[a]Cellular Organization and Signalling, National Centre for Biological Science, Tata Institute for Fundamental Research, Bangalore 560 065, India; and [b]Institute for Stem Cell Research and Regenerative Medicine, Bangalore 560 065, India

Contributed by Satyajit Mayor, September 23, 2016 (sent for review June 29, 2016; reviewed by Marcos González-Gaitán and Ben-Zion Shilo)

Endocytosis of ligand-receptor complexes regulates signal transduction during development. In particular, clathrin and dynamin-dependent endocytosis has been well studied in the context of patterning of the *Drosophila* wing disc, wherein apically secreted Wingless (Wg) encounters its receptor, DFrizzled2 (DFz2), resulting in a distinctive dorso-ventral pattern of signaling outputs. Here, we directly track the endocytosis of Wg and DFz2 in the wing disc and demonstrate that Wg is endocytosed from the apical surface devoid of DFz2 via a dynamin-independent CLIC/GEEC pathway, regulated by Arf1, Garz, and class I PI3K. Subsequently, Wg containing CLIC/GEEC endosomes fuse with DFz2-containing vesicles derived from the clathrin and dynamin-dependent endocytic pathway, which results in a low pH-dependent transfer of Wg to DFz2 within the merged and acidified endosome to initiate Wg signaling. The employment of two distinct endocytic pathways exemplifies a mechanism wherein cells in tissues leverage multiple endocytic pathways to spatially regulate signaling.

clathrin and dynamin-independent endocytosis | Wingless signaling | pH of endosome | wing disc development | Garz localization

Wnts are a class of secreted proteins necessary for patterning and growth at multiple steps throughout development (1, 2). Wnt-mediated signaling and morphogenesis has been well studied in *Drosophila* wing discs, wherein the Wnt protein, Wingless (Wg), interacts with a seven-pass transmembrane receptor, DFrizzled2 (DFz2), and a coreceptor, Arrow, to trigger the canonical Wg-signaling cascade and elicit β-catenin–based transcriptional responses (3, 4).

Wg, secreted at the dorso-ventral (D/V) boundary, forms a spatial gradient across the boundary and activates distinct concentration-dependent transcriptional programs ensuing coordinated tissue growth (5, 6). This process necessitates a fine-tuning of morphogen-mediated signaling. It has been argued that these signals depend on cellular processes, such as secretion of the ligand, interaction of the ligand with cognate signaling receptors, and degradation of the ligand–receptor complex for the termination of signaling. The latter is often mediated by the endocytosis of morphogens (7, 8). Cellular parameters governing these processes need to be quantitatively determined to understand the generation and the interpretation of patterning signals, such as Wg.

Trafficking of Wg in the producing cells and the receiving cells is important for Wg signal transduction. In the producing cells, Wg is palmitoylated in the endoplasmic reticulum and trafficked to the plasma membrane with the assistance of Wntless and the retromer complex. Perturbation of any of these processes leading to Wg secretion results in both accumulation of Wg within the producing cells and reduction of Wg signaling in the receiving zone of the wing disc (9, 10). Endocytosis in the signal-receiving cells may either be important in shaping the distribution of secreted Wg across the wing disc (11) or in a cell-autonomous fashion affect signaling by promoting the interaction of Wg and DFz2 within an endosome (12, 13). Endocytosis also mediates Arrow-directed degradation necessary for the observed Wg distribution and signaling (14). However, rescue of patterning is observed even upon replacement of the endogenous Wg with a transmembrane-tethered Wg, thus raising questions on the importance of a secreted Wg gradient (15). Regardless, inhibition of endocytosis in the recipient cells, by using the dominant-negative (DN) or the temperature-sensitive form of *shibire*, demonstrates the importance of dynamin-dependent endocytosis in Wg-mediated signaling (11, 13). Interestingly, when examined carefully, Wg is observed in endosomes even in null clones of its signaling receptors Frizzled (Fz) and Arrow (14, 16–17), suggesting that other receptors or pathways may be important for its internalization.

Apart from its signaling receptors, a class of cell-surface molecules that influence Wg distribution and signaling are the glycosylphosphatidylinositol (GPI)-anchored heparan sulfate proteoglycans (HSPGs), Dally and Dlp. Whereas Dally positively contributes to Wg signaling (18), Dlp has a biphasic effect on Wg signaling depending on its concentration (19). GPI-anchored proteins are predominantly endocytosed by a clathrin and dynamin-independent CLIC (clathrin-independent carriers)/GEEC (GPI-anchored protein enriched endosomal compartments) pathway (henceforth referred to as the CG pathway) (20, 21). This pathway is regulated by small GTPases, Arf1 (Arf 79F in *Drosophila*) and Cdc42, the guanine nucleotide exchange factor (GEF) of Arf1 called GBF1 (*garz* in *Drosophila*), and is sensitive to both plasma-membrane composition and requires dynamic actin (22–24). The interaction of Wg with GPI-anchored HSPGs, as well as its ability to be endocytosed in a Fz-independent manner, prompted us to reexamine Wg internalization.

Significance

Regulated interaction of secreted morphogens with their receptors is necessary for patterning of tissues during development. The morphogen Wingless (Wg) is apically secreted at the dorso-ventral boundary of *Drosophila* wing imaginal discs, and its receptor, DFrizzled2 (DFz2), is localized basally in recipient cells. Here, we show that Wg is endocytosed by a dynamin-independent endocytic pathway, the CLIC/GEEC pathway, at the apical surface of the epithelium, whereas DFz2 is internalized basally via the conventional clathrin-dependent mechanism. Subsequently, Wg requires the acidic milieu of the merged endosome derived from the fusion of these two pathways to interact with DFz2 for subsequent signaling. This study provides evidence for a mechanism wherein cells leverage multiple endocytic pathways to coordinate signaling during patterning.

Author contributions: A.H. and S.M. designed research; A.H. performed research; A.H. contributed new reagents/analytic tools; A.H. and C.P. analyzed data; and A.H., C.P., and S.M. wrote the paper.

Reviewers: M.G.-G., University of Geneva; and B.-Z.S., Weizmann Institute of Science.

The authors declare no conflict of interest.

Freely available online through the PNAS open access option.

[1]To whom correspondence should be addressed. Email: mayor@ncbs.res.in.

This article contains supporting information online at www.pnas.org/lookup/suppl/doi:10.1073/pnas.1610565113/-/DCSupplemental.

On studying the trafficking of Wg and DFz2 in the *Drosophila* wing discs by directly labeling the endosomes of Wg and DFz2, we observed distinct early endosomes carrying either Wg or DFz2 with Wg endosomes enriched in the apical surface, whereas DFz2 endosomes were concentrated in the basal part of the wing disc. Although endocytosis of DFz2 is sensitive to dynamin, we found that Wg is endocytosed in a dynamin-independent manner. Furthermore, we characterized this dynamin-independent internalization route of Wg as being sensitive to perturbation of Arf1, Garz, and class I PI3K. Fusion of endosomes derived from these two distinct endocytic pathways facilitates the interaction of Wg and DFz2 within endosomes. Using FRET, we found that the low-pH milieu of the early endosome promotes the interaction between Wg and DFz2. Like the effects of perturbation of the clathrin and dynamin-dependent (CD) pathway on Wg signaling, inhibition of CG-mediated endocytosis of Wg reduces signaling in the wing disc and in *Drosophila* cell lines. These results provide evidence for a critical in vivo role for the dynamin-independent CG pathway. In addition, this mechanism, wherein the ligand and receptor are separately internalized and interact within an endosome, provides a paradigm for signal regulation that may be exploited in other signaling contexts.

Results

Wg Is Internalized Apically Devoid of Its Signaling Receptor, DFz2. We first examined the endocytosis of Wg and DFz2 in wing discs from third-instar larvae. For this purpose, we used fluorescently conjugated primary antibodies that enabled us to directly visualize these molecules at the cell surface, and in endosomes without any loss as a result of cell permeabilization (assay depicted in Fig. 1*A* and described in *SI Materials and Methods*). A monoclonal antibody against Wg and two primary antibodies against the extracellular domain of DFz2 were used. *SI Materials and Methods* and Fig. S1 *A* and *B* describe the specificity of the monoclonal antibody raised against N-terminus DFz2; the polyclonal antibody is described previously (25).

Cell-surface staining (assay depicted in Fig. 1*A*, step 1) shows that extracellular Wg and DFz2 have opposing distributions in the wing pouch, with Wg concentrated near the D/V boundary and DFz2 at the edges of the wing pouch (Fig. S1*C* and Movie S1). DFz2 is also localized primarily at the baso-lateral regions of the wing disc (26), whereas Wg is found both apically and baso-laterally. We next tracked the endocytosis of cell surface-labeled Wg and DFz2 for different time points. At early times postinternalization (5 min after endocytosis and after a quantitative removal of cell-surface fluorescence; assay depicted in Fig. 1*A*, step 3), Wg and DFz2 endosomes are also spatially segregated. Wg and DFz2 endosomal distribution mirrors the corresponding cell-surface distribution across the D/V boundary; Wg endosomes are near the D/V boundary and DFz2 endosomes are enriched toward either edges of the wing pouch. Furthermore, Wg endosomes are enriched in the apical surface, whereas DFz2 endosomes are accumulated near the basal surface (Fig. 1*B*, apical and basal, Fig. S1*D*, and Movie S2). Strikingly, in regions where Wg and DFz2 endosomes are present in the same region of the wing disc, these molecules appear in distinct endosomes (colocalization index: 10 ± 7% at a single plane, n = 15–20 fields each from three wing discs), in distinct subcellular localizations (Fig. 1 *B* and *C*, away from D/V). These apically localized Wg early endosomes colocalize extensively with the fluid-phase, monitored by incubation with fluorescently labeled dextran (Dex), a marker of the clathrin and dynamin-independent CG pathway of endocytosis (Fig. 1 *B* and *C*) (colocalization index at a single confocal plane: 83.08 ± 13%, n = 10–15 fields each, from three wing discs) (20). Although Dex endosomes are also found in the baso-lateral planes where DFz2 endosomes are abundant, they are found in distinct vesicles (colocalization index: 11.63 ± 3.37%, n = 10–15 fields each from four wing discs) (Fig. 1*D*). Thus, a large fraction of Wg and DFz2 appear to be internalized independent of each other.

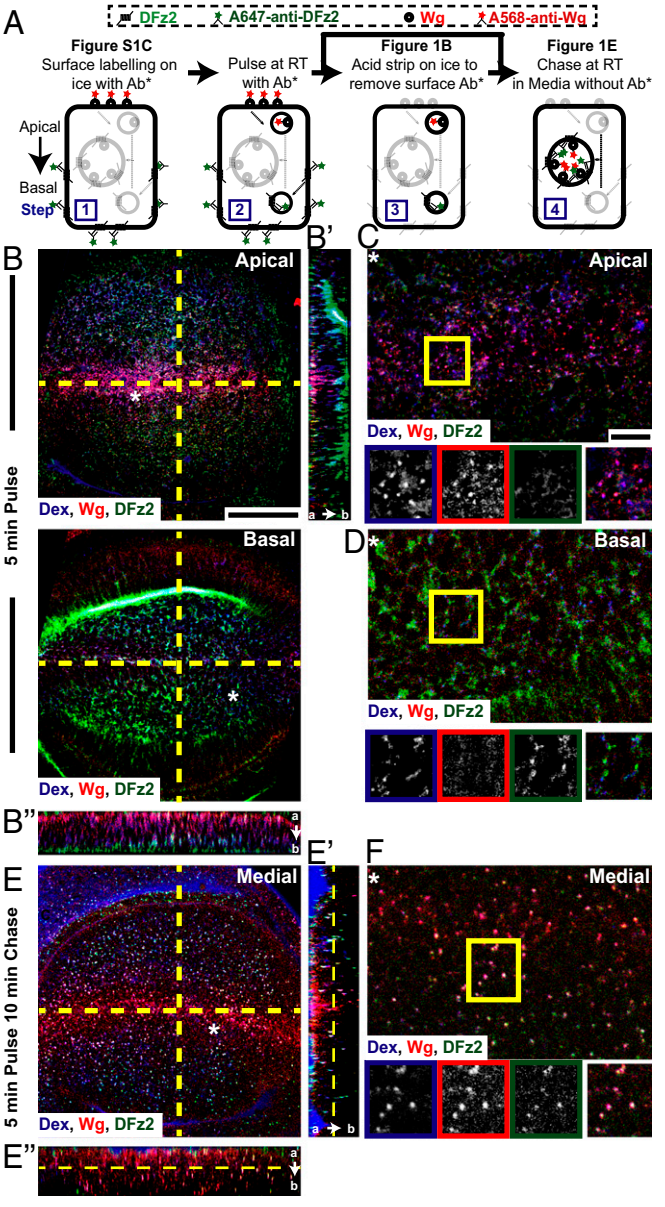

Fig. 1. Wg is endocytosed apically devoid of its signaling receptor, DFz2. (*A*) Endocytic assay: Surface distribution of Wg and DFz2 evaluated by incubating fluorescently labeled primary antibodies (Ab*) A568-anti-Wg, A647-anti-DFz2 on ice (step 1) (Fig. S1*C*). Surface-labeled wing discs are incubated at room temperature for 3–5 min with Ab* and Dex to image early endosomes (step 2) and acid washed to remove the Ab* left at the surface (step 3; see *B–D*), followed by chase in media without Ab* (step 4; see *E* and *F*). (*B–F*) Apical (*B*, *Upper*) and basal (*B*, *Lower*) confocal sections of control (w^{1118}) wing discs shows "5-min pulse" endosomes (*B*) and the medial plane of w^{1118} wing discs shows "5-min pulse and 10-min chase" endosomes (*E*) of Dex (blue), Wg (red), and DFz2 (green). YZ (*B′*/*E′*) and XZ (*B″*/*E″*) sections (along yellow lines in *B* and *E*) are oriented apical to basal (a → b). Regions (*) from *B* and *E* are magnified in *C*, *D*, and *F*. Boxed regions (*C*, *D*, and *F*) are magnified (~1.5×) and shown below with indicated probes in the color outlines. Images have been rotated (*B–D*), background-subtracted, and median-filtered with intensities appropriately scaled. Wg and Dex colocalize extensively in apical endosomes, whereas DFz2 endosomes are predominantly found basally, yet separate from Dex endosomes 5-min postinternalization. With time, all three colocalize in a common endosome in more medial planes. (Scale bars, 50 μm in *B* and *E* and 10 μm in *C*, *D*, and *F*.)

In contrast, after 15 min (Fig. 1*E*, Fig. S1*E*, and Movie S3; assay depicted in Fig. 1*A*, step 4), Wg, DFz2, and Dex all colocalize in large endosomal compartments along the apico-basal axis of the

wing disc. Although the distribution of Wg and DFz2 endosomes still oppose each other along the wing pouch, DFz2 colocalizes extensively with Wg in endosomes adjacent to the D/V boundary (Fig. 1*F*) (colocalization index: 78 ± 12%, n = 15–20 fields each from two wing discs). Typically, vesicles derived from distinct endocytic pathways are initially observed as separate endosomes carrying characteristic cargoes. Subsequently, the vesicles undergo heterotypic fusion and mature into Rab5^{+}-sorting endosomes, from where cargoes can either be recycled or degraded (27). The merged early endosomes containing Wg and DFz2 (10–15 min) in the wing disc are also positive for Rab5 GFP (Fig. S1 *F–H*), an early endosomal marker (28, 29). Hence, these endosomes probably act as sites of colocalization and concentration of Wg and DFz2, even in regions where their surface concentrations are low.

Wg Internalization Does Not Require Dynamin. Perturbation of CD endocytosis by using temperature-sensitive mutants or DN mutants of *shibire* (fly homolog of *Dynamin*) was found to affect Wg signaling in wing discs (11, 13). To characterize the DFz2-independent internalization route of Wg, we examined the extent of endocytosis of DFz2 and Wg in wing discs of the temperature-sensitive mutant *shibire*^{ts1} (*shi*^{ts1}) larvae after incubating them at restrictive temperatures (31–32 °C) for a short interval of time (15 min). In addition, we also monitored the uptake of Dex, to monitor the clathrin and dynamin-independent CG pathway, and fluorescently labeled maleyated BSA (mBSA), a ligand for scavenger receptors to monitor CD endocytosis (30) to evaluate endocytic activity in wing discs of *shi*^{ts1} larvae. Incubation at restrictive conditions inhibits both DFz2 endocytosis (Fig. 2 *A*, *B*, and *E*) and mBSA endocytosis (compare Fig. S2 *A′* and *B′*), whereas Wg endocytosis (Fig. S2*F*; compare with Fig. 2 *C*, *D*, and *F*) and fluid-phase uptake (compare Fig. S2 *A* and *B*) are not reduced; and in fact, it appears to be slightly enhanced at the restrictive temperatures. Upon shifting the *shi*^{ts1} wing discs to restrictive temperatures, DFz2 extracellular staining was similar to control discs, indicating that the reduced endocytosis is because of a block in the endocytic pathway (Fig. S2 *D* and *E*). However, it should be noted that longer incubations of *shi*^{ts1} wing discs at restrictive temperatures (32 °C for 40 min) results in complete inhibition of both endocytic pathways as evaluated by monitoring Dex and mBSA endocytosis (Fig. S2 *C* and *C′*), probably because of the other secondary effects of dynamin inhibition (30). *shi*^{ts1} is a rapidly acting temperature-sensitive allele of dynamin, characterized by its almost instantaneous paralytic phenotype (3 min) at temperatures above 29 °C (31). Within minutes of exposure to restrictive temperatures, arrested pits accumulate at presynaptic membranes of these flies (32). Although its rapid inactivation kinetics make it a convenient tool, *shi*^{ts1} flies recovered much slower than other *shibire* mutants and recovery time was correlated to the length of heat shock, indicative of an effect on this allele on dynamin aggregation (33) and possibly other secondary effects, with prolonged incubations at restrictive temperature. Hence, all experiments on *shi*^{ts1} were done at incubation time up to 15 min, wherein the markers of CG endocytosis were internalized but CD cargo was inhibited.

Together with the observation that Wg continues to be endocytosed in clones of cells in wing discs that lack Fz1 and DFz2 (Fig. S1*I*) (see also refs. 14, 16, and 17), these results indicate that a large fraction of Wg is internalized by a dynamin-independent endocytic pathway, independent of its signaling receptor, DFz2.

Wg Is Internalized via a Garz-Mediated Endocytic Pathway in *Drosophila* Wing Disc. The dynamin-independent endocytosis of Wg prompted us to explore the roles of mediators of such an endocytic pathway in *Drosophila*. It is likely that Arf79F, along with its GEF Garz, functions in the formation of vesicles in dynamin-independent CG endocytosis (22, 24). We expressed interference RNA (RNAi) against Arf79F and Garz using the following specific GAL4 drivers: C5GAL4, which is expressed in cells of the wing disc that signal in response to Wg but not in cells that produce Wg (13), and

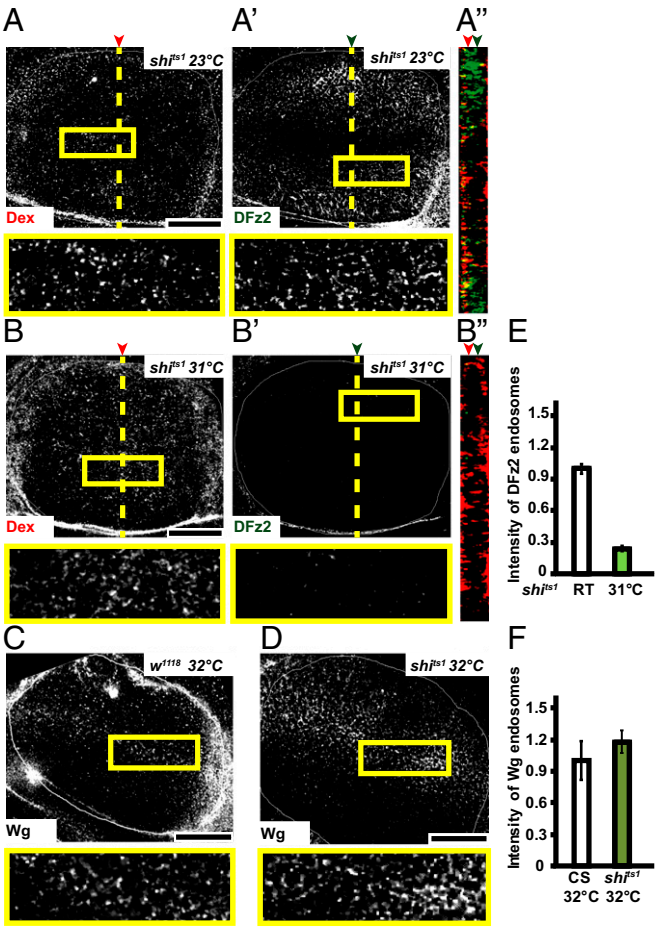

Fig. 2. *Shibire* is not required for Wg endocytosis. (*A–F*) Confocal sections of wing discs from *shi*^{ts1} (*A*, *B*, and *D*) or *w*^{1118} (*C*) incubated at the permissive temperature of 23 °C (*A* and *C*) or at the restrictive temperature of 31–32 °C (*B* and *D*) showing 5- to 8-min pulsed endosomes of Dextran (*A* and *B*; red in *A″* and *B″*), DFz2 (*A′* and *B′*; green in *A″* and *B″*), or Wg (*C* and *D*). *E* and *F* show quantification of the intensity of DFz2 and Wg endosomes, respectively, between control and *shi*^{ts1} wing discs. Robust endocytic uptake of fluid and mBSA is observed in wing discs of *w*^{1118} (32 °C) and *shi*^{ts1} (room temperature-permissive) and both serve as controls for Dynamin function. Error bars indicate the SE calculated from three to six wing discs. $P < 10^{-25}$ in *E*. *A″* and *B″* indicate YZ projection of Control and *shi*^{ts1} wing discs, respectively, along the planes indicated. Red and green arrows in *A″* and *B″* indicate the plane of the representative images. Boxed regions are magnified (~2.7×) and shown below the respective images. The image in *C* has been rotated; all images background-subtracted and median-filtered with intensities appropriately scaled for representation. Although DFz2 endocytosis is affected in *shi*^{ts1} wing discs shifted to restrictive temperature, both Dex and Wg endocytosis remain unaffected. (Scale bars, 50 μm.)

Hedgehog GAL4 (HhGAL4), which is expressed only in the posterior compartment of the wing disc (Fig. S3 *A* and *B*).

Expression of Garz RNAi in HhGAL4 domain for 36–40 h greatly reduces the extent of fluid-phase endocytosis in the posterior compartment as visualized by monitoring the uptake of Dex (Fig. 3*A′*), whereas in the same cells, the CD pathway—monitored by the uptake of mBSA—is not reduced (Fig. 3*A*). We verified the viability of wing disc cells depleted of Garz and observed no alterations in localization of cell polarity marker (Dlg) or aberrant apoptosis (Fig. S3 *C*, *D*, and *D′*). Immunostaining against the Garz protein confirmed the knockdown in the posterior compartment compared with the control anterior compartment (Fig. S3*E*). A similar reduction in the CG pathway, but not in the CD pathway, is observed in C5GAL4 driven Garz RNAi wing discs (Fig. S3 *F* and

F′). In addition, consistent with our previous results (24, 34), when *Drosophila* S2R+ cell lines carrying the human transferrin receptor (CD cargo) is treated with Garz dsRNA, CG endocytosis is selectively reduced without perturbing transferrin endocytosis (Fig. S3 *G* and *G′*). Thus, Garz RNAi expression in the wing disc under the conditions of knockdown, detailed above and in *Drosophila* cell lines, inhibits endocytosis via the CG pathway.

Wg endocytosis is also reduced by ∼60% (Fig. S3*H*) in the posterior half of wing discs expressing Garz RNAi, driven using HhGAL4 in the posterior domain, compared with corresponding uptake in cells in the anterior compartment (Fig. 3*C*). In contrast, DFz2 internalization appears unaffected by the expression of Garz RNAi, because endosomes are uniformly distributed across both anterior and posterior domains (Fig. 3*D* and Fig. S3*H*). The fluid-phase uptake in both these wing discs (Fig. 3 *C* and *D*) continues to be significantly reduced (by ∼55%) (Fig. S3*H*) in the posterior compartment compared with the anterior (Fig. S3 *H–J*).

Reduced numbers or intensities of Wg endosomes can either be because of reduced amount of Wg available at the cell surface or because of a deficient endocytic machinery. To distinguish these two possibilities, we estimated the amount of extracellular Wg and calibrated the extent of endocytosis using a surface internalization assay (*SI Materials and Methods*). We observe that the extracellular levels of Wg are not reduced upon Garz depletion in the posterior compartment (HhGAL4) (Fig. 3 *F* and *G*) or in the wing pouch (C5GAL4) (Fig. 3*H*), unlike Arf 79F depletion in similar conditions, which affects secretion and hence the extracellular levels of Wg (Fig. 3*E*). Other GEFs could be compensating for Garz function under these conditions at the Golgi. Furthermore, a quantitative surface internalization assay that estimates the extent of Wg endocytosed normalized to extracellular Wg (Fig. 1*A*, steps 1 and 2, and *SI Materials and Methods*) shows that whereas control discs exhibit robust Wg uptake, C5GAL4-driven Garz RNAi discs show significantly reduced Wg uptake (Fig. 3 *H*, *H′*, and *I*). Together, these results demonstrate that Garz depletion neither affects DFz2 endocytosis via the CD pathway nor reduces the extracellular levels of Wg; however, it severely perturbs the internalization of Wg.

Class I PI3K Aids in Localization of Garz to the Plasma Membrane and Specifically Alters Endocytosis of the Fluid Phase and Wingless. The roles of Garz and Arf1 have also been associated with the regulation of secretion (35, 36). For example, the expansion of tracheal tubes during *Drosophila* embryogenesis is dependent upon Arf79F, Garz, and the ArfGAP–Gap69C regulated retrograde trafficking of Coatomer (COPI)-coated vesicles from the Golgi to the endoplasmic reticulum (37). Although the titrated knockdown of Garz did not alter the levels of extracellular Wg (Fig. 3*F*) or DFz2 (see, for example, Fig. S5*B*), knocking down Arf79F using the same GAL4 system indeed reduces the extracellular levels of Wg in the posterior half of the wing disc (Fig. 3 *E* and *G*), consistent with a role for Arf79F in secretion of Wg in the wing disc. Localization of Garz and Arf1 to the Golgi or plasma membrane in a dynamic

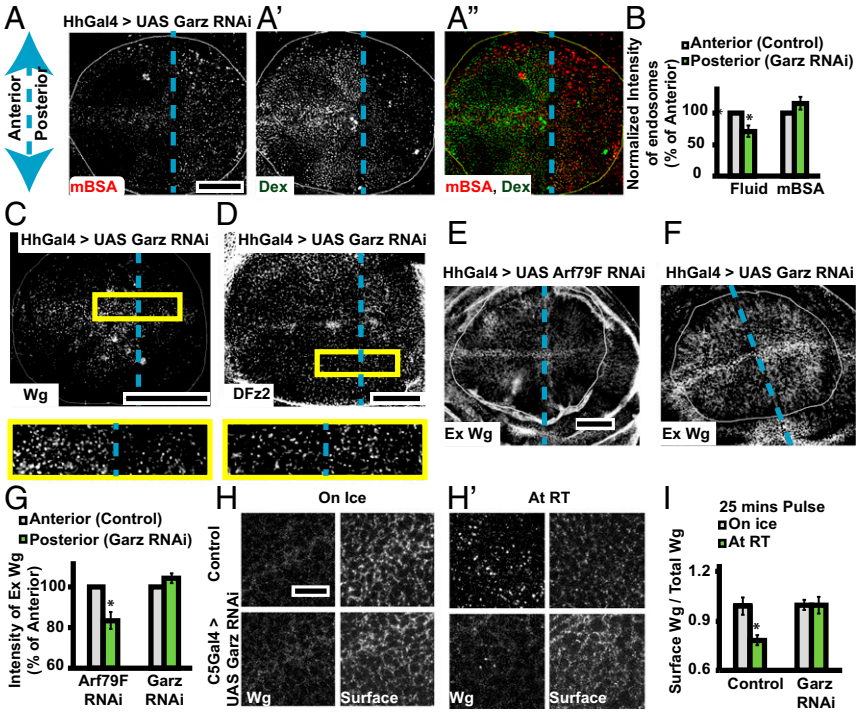

Fig. 3. Garz perturbation specifically affects fluid phase and Wg endocytosis. Dashed blue line indicates the anterior/posterior (A/P) compartment boundary. Posterior is to the right in all disc images. (*A*) Confocal projections of wing discs with HhGAL4 driving Garz RNAi in the posterior showing: 15-min endocytosis of CD cargo–mBSA (*A*; red in merge), Dex (*A′*; green in merge), and merge (*A″*); 10-min endocytosis of Wg (*C*; Dex uptake in Fig. S3*I*) and DFz2 (*D*; Dex uptake in Fig. S3*J*). Histogram in *B* represents the normalized (to the compartment area) intensity of Dex and mBSA endosomes in the posterior with respect to the anterior ($n = 6$ wing discs). Yellow boxes (*C* and *D*) are magnified (∼2.5×) below. Images are average intensity projections of confocal planes (13 planes in *A*; 3 apical planes in *C*; and 3 basolateral planes in *D*; depth, 1.0 μm). Although Wg and fluid (Dex) endocytosis is severely reduced in the posterior with respect to the anterior, DFz2 and mBSA endocytosis is not. (*E–G*) Confocal projections (six to eight confocal planes; depth, 1.0 μm) of extracellular Wg staining in wing discs with Arf79F RNAi (*E*) or Garz RNAi (*F*) driven in the posterior compartment with HhGAL4. Histogram (*G*) shows that the surface levels of Wg is not reduced across A/P axis upon depletion of Garz, unlike Arf79F depletion. (*H–I*) Surface internalization assay (*SI Materials and Methods*) using A568 anti-Wg (1° antibody-Wg) and A647 anti-mouse (2° antibody-surface) on control wing discs (*H*, *Upper*) and those with Garz RNAi expressed under C5GAL4 (*H*, *Lower*): Confocal slices from wing discs maintained on ice/room temperature are represented as *H*/*H′*. Histogram in *I* shows the amount of 2° antibody bound after 25 min at the indicated temperature, normalized to the total 1° bound Wg initially present at the cell surface (*SI Materials and Methods*). $n = 5$ discs; 2 repeats; $^*P < 10^{-3}$. All images are background-subtracted, median-filtered (*A*, *C*, *D*) and intensities appropriately scaled. (Scale bars, 50 μm in *A–A″* and *C–F*, and 10 μm in *H* and *H′*.)

manner can determine its role in secretion or CG endocytosis. In neutrophils, it has been demonstrated that GBF1 (the mammalian homolog of Garz) bears a lipid binding motif necessary for binding to the products of PI3Kγ. The activity of PI3Kγ assists in the translocation of GBF1 from the Golgi to the leading edge of the cell upon G protein-coupled receptor stimulation (38). To further understand the role of Arf1 and Garz in Wg uptake, we examined the role of class I PI3K in Garz localization and in the CG pathway.

To test for the role of class I PI3K in Garz localization, we expressed a GFP-tagged Garz construct (37) in the larval fat bodies (Fig. 4 *A–D* and Fig. S4 *A* and *B*) and in the wing disc (Fig. S4 *C–F*) and evaluated its localization upon treatment with PI3K inhibitor (LY294002), which inhibits class I PI3K (39, 40). GFP–Garz colocalizes with both FM dye-labeled plasma membrane (Fig. 4*A*) and with the Golgi-marker GM130 (Fig. 4*C*). Upon treatment with LY294002, the recruitment of Garz to the plasma membrane is lost (Fig. 4*B*) and GFP–Garz is redistributed to vesicular structures, which remain colocalized with GM130 (Fig. 4*D*). LY294002 also appears to have an effect on the distribution of GM130-labeled Golgi structures. Despite this finding, Garz–GFP remains strongly colocalized with GM130. This is specific because there is no global redistribution of cytosolic GFP on treatment with LY294002 (Fig. S4 *A* and *B*). Even in wing discs, GFP–Garz is localized to plasma membrane and upon addition of PI3K inhibitor, LY294002, the ratio of GFP–Garz intensities at the cell boundary to that in the cell interior reduces (Fig. S4 *C–F*). Furthermore, in S2R+ cells overexpressing GFP–Garz we evaluated the changes in plasma membrane localization upon treatment with both LY294002 or dsRNA depletion of catalytic subunit of class I PI3K (Dp110). The measurement of total internal reflection fluorescence (TIRF)/epifluorescence intensity ratios provides an assay for the loss or enrichment of fluorescently tagged proteins at the plasma membrane. This ratio is drastically reduced for GFP–Garz (Fig. 4 *E* and *E′*) in both the treatments, whereas a control construct (myristoylated GFP, Myr-GFP) showed no difference (Fig. 4 *F* and *F′*). Thus, localization of Garz to the plasma membrane is dynamic and requires the activity of class I PI3K.

Depletion of PI3K21B, the regulatory subunit of class I PI3K, in the wing disc using HhGAL4, also leads to specific reduction of fluid-phase and Wg endocytosis in the posterior region (Fig. 5 *A* and *A′*). However, depletion of PI3K21B (using the same driver) did not reduce DFz2 endocytosis (Fig. 5 *B* and *B′*); DFz2 endosomes are in fact slightly more in number in the posterior compartment compared with the anterior compartment. Endocytosis of DFz2 in the posterior compartment, where PI3K 21B RNAi is driven, is enhanced by ~30% (Fig. 5*B*) [132.6 ± 8.9% endocytosis in the posterior compartment compared with that in the anterior compartment (set to 100%); $n = 7$ wing discs]. Similarly, in S2R+ cells depleted of PI3K21B, Dex uptake is greatly reduced, whereas CD endocytosis (transferrin uptake) is somewhat enhanced (Fig. 5 *C* and *D*). These results implicate class I PI3K in regulating the localization of Garz at the plasma membrane and its loss-of-function inhibits CG endocytosis of Wg.

Perturbation of Garz and Class I PI3K Affects Wingless Signaling. The results thus far show that Wg is endocytosed via the CG pathway, independent of its signaling receptor DFz2 and, furthermore, perturbation of regulators of the CG pathway (Garz, class I PI3K) inhibits Wg endocytosis, but not DFz2 endocytosis. We therefore tested the role of CG endocytosis in Wg signal transduction. Wg signaling output in the wing disc can be monitored by assessing the levels of two transcriptional readouts: a short-range signaling output, Senseless, and a long-range signaling output, Distalless (5, 41). These targets of Wg are drastically reduced in wing discs where Garz RNAi is driven with C5GAL4 (Fig. 6*A* and Fig. S5 *F–H*) and HhGAL4 (Fig. 6*B* and Fig. S5 *A* and *I*). This reduction in Wg signaling is not because of any alterations in the extracellular levels of Wg (Fig. 3 *F* and *G*) or DFz2 measured (Fig. S5*B*) across

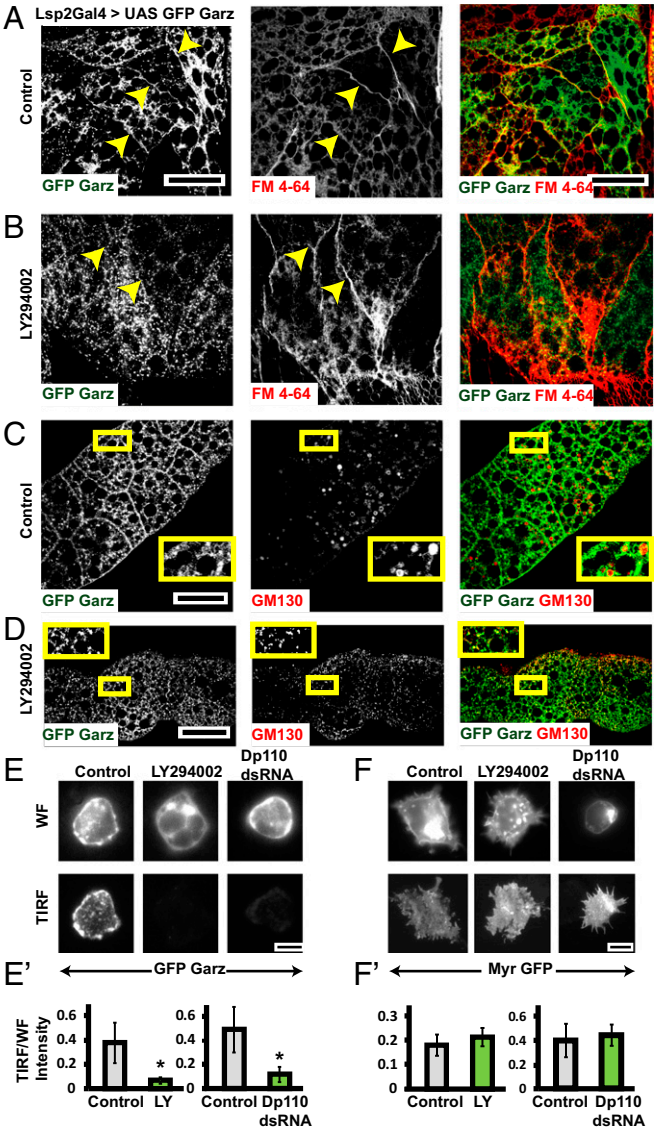

Fig. 4. Class I PI3K mediates plasma membrane localization of Garz. (*A–D*) Confocal slices of UAS-GFP Garz (*A–D*; green) expressed in fat bodies using LSP2 GAL4 showing marked accumulation (*A*) along the plasma membrane labeled by FM4-64 dye (red) and (*C*) in Golgi labeled by GM130 (red). Upon treatment with LY294002 the plasma membrane localization of GFP–Garz is lost (*B*), but the Golgi localization appears unaffected (*D*). Yellow arrows in *A* and *B* point toward plasma membrane. The outlined regions in yellow are magnified (~2.1×) and shown as *Insets* in *C* and *D*. (*E* and *F*) TIRF and widefield (WF) images of S2R+ cells expressing Actin GAL4 and pUAST-GFP–Garz (*E*) or pUAST-myristoylated-GFP (*F*) in untreated (Control) or cells treated with LY294002 or Dp110 dsRNA. The ratio of TIRF/WF, which reflects the relative extent of membrane localization of the protein, is plotted in *E′* and *F′*. Although the ratio of GFP–Garz reduces in both the PI3K perturbed conditions (*$P < 0.2 \times 10^{-3}$), the ratio of myr GFP (although these cells are more spread with many filopodia) is not significantly different between the wild-type and perturbations. All images are background-subtracted and intensities appropriately scaled for representation. (Scale bars, 50 μm in *A–D* and 10 μm in *E* and *F*.)

the disc, and is similar to that of depletion of Arrow (Fig. S5*K*). The reduction in Wg signaling is specific, because the levels of Cubitus interruptus, a signaling readout of another secreted morphogen, Hedgehog, remains unaffected upon Garz depletion (Fig. S5 *C–E*).

In S2R+ cell lines, treatment with Garz dsRNA, as well as expression of the Garz DN mutant E740K mutation in the GEF

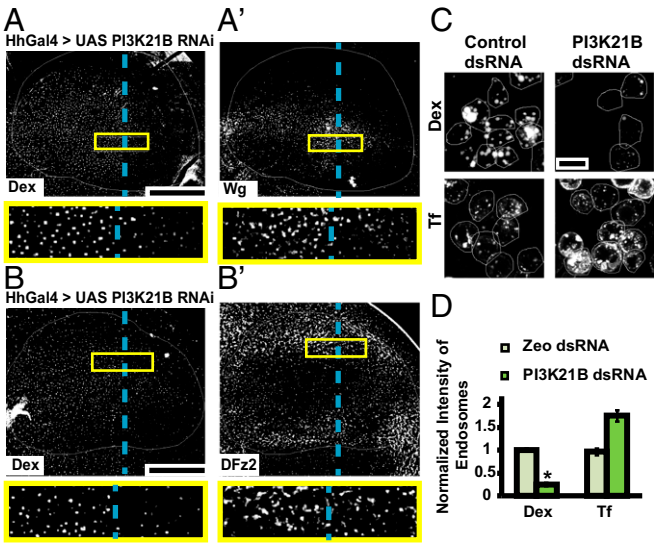

Fig. 5. PI3K perturbation specifically affects fluid phase and Wg endocytosis. (*A* and *B*) Confocal images of wing discs expressing PI3K21B RNAi using HhGAL4 in the posterior compartment showing 10-min endosomes of (*A* and *A′*) Dex and Wg, and (*B* and *B′*) Dex and DFz2, probed using FITC-Dex and A568 anti-Wg or A647 anti-DFz2. Both Wg and Dex uptake is reduced in the posterior compartment compared with the control anterior side, whereas DFz2 endosomes are similar in the posterior compared with anterior. Images are average intensity projections of confocal planes (10 apical planes in *A*; 7 apical planes in *B*; 7 basolateral planes in *B′*), each of depth 1.0 μm with background-subtraction and median-filtering and intensities appropriately scaled for representation. The outlined regions in yellow are magnified (~3.7×) and shown below respective images. Posterior compartment is to the right in all wing discs. Dashed blue line approximately indicates the A/P compartment boundary. (*C* and *D*) WF images of S2R+ cells with control (Zeocin) or PI3K21B dsRNA showing 10-min uptake of Dex (*C*, *Upper*) and transferrin (*C*, *Lower*). Dex uptake is reduced whereas transferrin uptake is slightly enhanced in PI3K21B dsRNA cells as quantified in the histogram (*D*). $*P < 10^{-20}$ obtained from 80 to 100 cells with two replicates. Images are background subtracted and intensities are appropriately scaled for representation. (Scale bar, 50 μm in *A*, *A′*, *B*, and *B′* and 10 μm in *C*.)

domain (37), reduces Wg signaling, as evaluated by luciferase assays (42) (Fig. 6*C*). This finding is consistent with a cell-autonomous role for Wg endocytosis in activating β-catenin– (Armadillo) dependent Wg target genes. Furthermore, the reduction of signaling in S2R+ lines is rescued by the expression of dominant-active Armadillo (DA-Arm) (Fig. 6*D*). The GSK3-β inhibitor, SB216763 (43), inhibits phosphorylation and degradation of Armadillo, and therefore activates Wg signaling even in the absence of Wg. Addition of the GSK3-β inhibitor to cells treated with control or Garz double-stranded (ds)RNA results in luciferase activity similar to that in the control cells (Fig. 6*E*). Thus, Garz functions upstream of both GSK3-β and Armadillo in Wg signaling.

Concomitant with the inhibition of Wg endocytosis, Wg signaling is also severely reduced in the posterior domain of the wing discs where class I PI3K activity is perturbed. Driving of DN Dp110 (UAS-Dp110^{D954A}), RNAi against PI3K21B, and overexpression of PTEN [which dephosphorylates PI(3,4,5)P3 (phosphatidylinositol 3,4,5-trisphosphate, PIP3) to PI(4,5)P2 (PIP2)] using the HhGAL4; GAL80^{ts} system for 38–44 h also causes a reduction in Senseless (Fig. 6 *G*–*I*, and Fig. S5*J*). In all three perturbations, the concentration of PIP3 is likely to be affected and has an effect on Wg signaling.

Class I PI3K is a key player in insulin-mediated growth signaling (44). In mammalian cells and in certain cancers, PI3K signaling has been known to converge on Wg signaling downstream (45, 46); this is via the recruitment and activation of Akt, which inactivates GSK3-β and thus prevents degradation of β-catenin. In fact, expression of Akt enhances Wg-induced luciferase activity in response to Wg (Fig. 6*F*). To confirm that the loss of Wg signaling upon the reduction of class I PI3K activity is not the result of a general loss of Akt activity, we overexpressed Akt in the background of this perturbation. In cell lines, Wg signaling is significantly reduced by Dp110 RNAi and cannot be rescued by overexpression of Akt, but can be rescued by DA-Arm expression (Fig. 6*F*). In wing discs, overexpression of Akt with HhGAL4 for 40 h leads to expansion of the posterior domain with an increase in the levels of Senseless and Distalless near the margins and in the wing pouch (Fig. 6*J*). However, overexpression of Akt in conjunction with Dp110 DN, does not rescue the loss of Senseless by Dp110 perturbation, despite preserving the overgrowth phenotype of Akt overexpression in the posterior domain (Fig. 6*K*). This finding suggests a delicate balance between growth rates and signaling in generating a normal wing because gross up-regulation or down-regulation of the PI3K pathway simply increases/decreases the size of the wing (47). However, we cannot exclude the possibility that PI3K also affects Wg signaling via Akt repression.

Thus, the role of class I PI3K in Wg signaling is upstream of the action of Akt, and is likely to act via the ability of its product PIP3 in recruiting Garz to the plasma membrane. Together, these results indicate that alteration of endocytosis via the CG pathway is sufficient to reduce Wg signaling.

Endocytosis and Endosomal Acidification Is Necessary for Wingless and DFz2 Interaction. We reasoned that endocytosis via the CG pathway is necessary for enhancing the interaction of Wg and DFz2 in colocalized endosomes (Fig. 1*E*). We measured the extent of interaction between Wg and DFz2 at the cell surface and within endosomes by using a FRET methodology that relies on donor dequenching upon acceptor photobleaching (48). The increase in fluorescence of the pH-insensitive donor (Alexa 568, labeled anti-Wg) upon photobleaching of the pH-insensitive acceptor fluorophore (Alexa 647, labeled anti-DFz2) serves as a measure of FRET efficiency (48). We find that FRET efficiency between Wg and DFz2 is significantly higher in endosomes compared with that at the cell surface, as measured in clusters from subapical and lateral regions of wing disc cells wherein the colocalization of Wg and DFz2 (Fig. 1*E*) at the cell surface is the highest (Fig. 7 *A*, *B*, and *D*). We further reasoned that the acidic milieu of the endosome may promote this interaction. Indeed, when measured, the pH of the early endosome in the wing discs is about 6.2 (Fig. S6*A*), and inhibition of vacuolar ATPases with Bafilomycin (Baf) (49) increases the pH of these endosomes to that of the extracellular buffer (7.2) (Fig. S6*A*). Baf-treated endosomes show a marked reduction in FRET, registering a value similar to that obtained at the cell surface (Fig. 7 *C* and *D*). This result also nullifies the trivial hypothesis that the higher FRET efficiency observed between Wg and DFz2 in an endosome is a result of enhanced concentration of Wg and DFz2 in the endosome, because Baf-treated endosomes are comparable in both size and intensities to that of untreated endosome, and yet registers a lower FRET efficiency. Interestingly, interfering with the acidification of the endosomes has also been reported to affect Wg signaling (50).

To ascertain if the acidic environment is sufficient to allow interactions between Wg and DFz2, we incubated wing discs in a low-pH buffer on ice (pH 6.0) immediately after labeling the surface Wg and DFz2 with their respective antibodies (*SI Materials and Methods*). Surface-labeled DFz2 and Wg (at pH 6.0) formed large clusters especially in the baso-lateral regions where DFz2 abounds (Fig. S6 *B* and *C*), and this is accompanied by an increase in average FRET efficiencies (Fig. 7 *E* and *F*).

Given that perturbations of both CG and CD endocytic pathways affect Wg signaling, we verified if endosomes are platforms for Wg signal transduction. We have previously shown that the fusion of the CG and CD pathway endosomes depend on Rab5 and a Wortmanin-sensitive class III PI3K (27). Knockdown of Class III

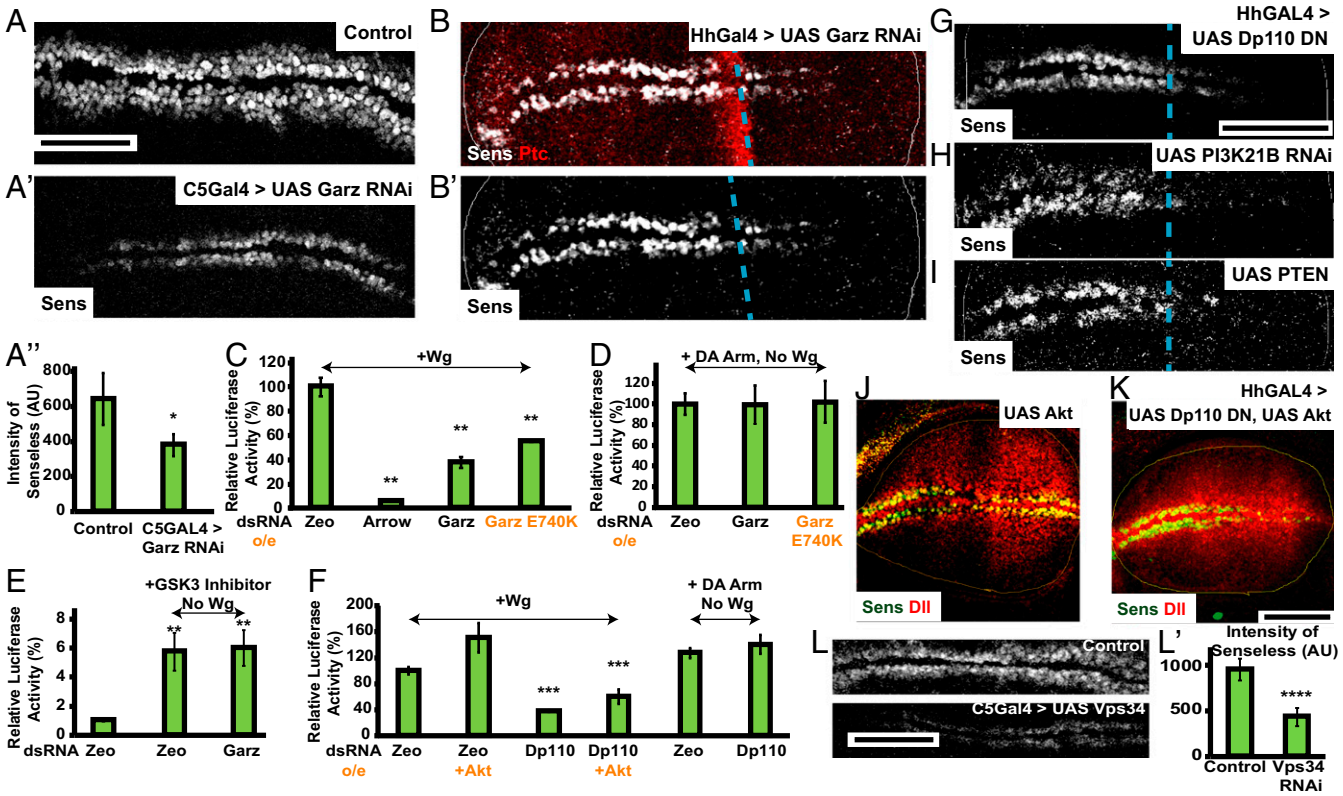

Fig. 6. Garz, class I PI3K, and vps34 perturbation affects Wg signaling. (*A* and *B*) Confocal images of Control (*A*, C5GAL4/+) and Garz RNAi (*A′*, C5GAL4 > GarzRNAi) wing discs and HhGAL4 driving Garz RNAi (*B*) wing discs immunostained for Senseless (the A/P compartment boundary is demarcated by Ptc staining). Histogram in (*A″*) shows the reduction in intensity of Senseless (Sens) quantified from 8 to 10 wing discs from the C5GAL4 > Garz RNAi discs. $*P < 10^{-7}$. Garz RNAi severely reduces expression Wg signaling output. (*C*–*F*) S2R+ cells were transfected with luciferase vectors STF16 and pDARL to evaluate roles of Garz and PI3K21B in Wg signal transduction. (*C* and *D*) Histograms show normalized Wg signaling in S2R+ cells treated with the indicated dsRNA or overexpressing (o/e) Garz E740K construct, evaluated after exogenous addition of Wg (*C*), or with coexpression of DA Arm and indicated treatments in the absence of exogenous Wg (*D*). Wg signaling in Arrow depleted cells is reduced to ∼5% of control, demonstrating the efficacy and dynamic range of the assay (42), Garz perturbations reduce Wg induced signaling but did not affect the extent of DA-Arm–induced signaling. Histogram (*E*) shows the extent of normalized Wg signaling in S2R+ cells treated with the indicated dsRNA and GSK3 inhibitor in the absence of exogenously added Wg. Note the induction of signaling by the addition of GSK3 inhibitor is insensitive to the effect of Garz dsRNA indicating that GSK3 functions downstream of Garz. Histogram (*F*) shows normalized Wg signaling in S2R+ cells induced by addition of exogenous Wg, and treated with the indicated dsRNA with or without overexpression of Akt. Note that Akt overexpression does not rescue the signaling defect of Garz, whereas signaling induced by DA Arm overexpression is insensitive to Dp110 depletion. Normalized luciferase values are represented as percent of control, and data are expressed as mean (±SEM) derived from two experiments. *P* values for all perturbations with respect to control: (in *C*–*E*) $**P < 10^{-5}$ and (in *F*) $***P < 10^{-3}$. (*G*–*K*) Perturbation of levels of PIP3 in the wing discs using overexpression of Dp110 DN (*G*), P13K21B RNAi (*H*), or overexpression of PTEN (*I*) in the posterior compartment for 36–40 h results in reduced Senseless expression. This signaling defect is not rescued by overexpression of Akt along with Dp110DN (Senseless in green, Distalless in red) as seen in *K*, whereas overexpression of both Akt alone (*J*) and Akt with Dp110DN (*K*) results in overgrown posterior compartment. Note that Akt overexpression alone doesn't cause any defects in Wg signal transduction. (*L*) Vps34, the class III PI3Kinase, when depleted using C5 GAL4 (*Lower*) reduces Senseless intensities compared with control (*Upper*) as quantified in *L′*. $****P < 10^{-15}$. All images are background-subtracted with intensities appropriately scaled for representation. Posterior compartment is to the right in all wing discs. Dashed blue line approximately indicates the A/P compartment boundary. (Scale bars, 50 μm.)

PI3K–Vps34 using C5GAL4 leads to defects in fusion of Wg and DFz2 endosomes (Fig. S7 *A* and *B*) and reduction in Wg signaling (Fig. 6 *L* and *L′*). However, as Vps34 also affects CD endocytosis (51), the effect on signaling could be because of a combination of endocytosis and merging defects.

If Wg signaling proceeds from endosomes, the downstream components of Wg signaling are expected to be localized to endosomes. Axin (using anti-Axin in Fig. S7*C*) and Dishevelled, two such Wg signaling components (Dsh; Dsh-GFP under its native promoter in Fig. S7*D*), were found in large vesicles colabeled by endosomal markers Hrs [29.3 ± 3.0% of Axin punctae colocalizes with Hrs in wing discs (Fig. S7*C*) and 57.93 ± 10.39% of Dsh GFP colocalizes with Hrs in S2R+ cells (Fig. S7*D*)]; Rab7 [20.91 ± 1.82% of Axin punctae colocalizes with Rab7 in wing discs (Fig. S7*C*) and 11.55 ± 8.24% of Dsh GFP colocalizes with Rab7 in S2R+ (Fig. S7*D*)]. Dsh-GFP also colocalized with early endosomes (∼5-min pulse) containing Wg (Fig. S7*E*) in S2R+ cells [45 ± 8.5% of Wg endosomes (5 min) strongly colocalizes with Dsh-GFP], whereas 10-min Dex endosomes in the wing disc, which are completely colocalized with Wg and DFz2 (Fig. 1*E*), are also decorated with Dsh-GFP [50.0 ± 3.1% of early endosomes containing tetramethylrhodamine (TMR)-Dex colocalizes with Dsh-GFP punctae] (Fig. S7 *F* and *F′*).

Conversely, to assess if DFz2 productively interacts with Wg at acidic pH, we determined if Dsh is recruited to the cell surface of wing discs upon changing pH. In the apical and subapical planes of control wing discs, where punctae of Dsh-GFP are clearly visible, the intensities appear to decrease across the D/V boundary (similar to the observed distribution of Wg). On the other hand, in acidic conditions, Dsh-GFP is uniformly distributed across the D/V boundary and higher levels of Dsh-GFP are observed as distinct punctae (Fig. 7 *G*–*I*). This finding indicates that if Wg–DFz2 interaction is fully enabled at the cell surface, there would be a productive engagement across the wing pouch and the loss of any

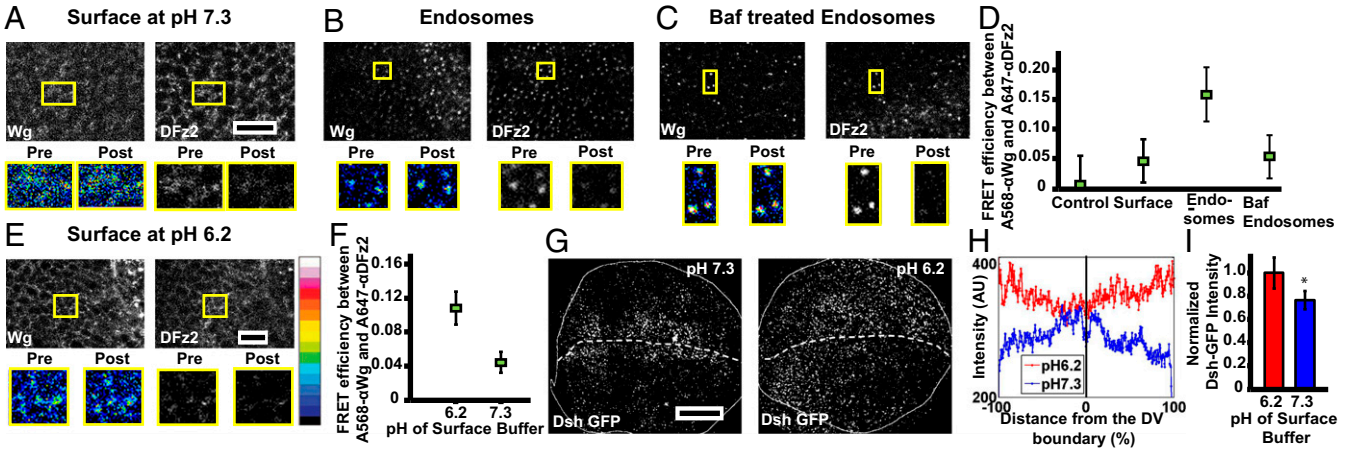

Fig. 7. Endosomal acidification is necessary for Wg–DFz2 interaction and signaling. (*A–C*) Confocal images of wing discs, surface labeled on ice with A568 anti-Wg and A647 anti-DFz2 (*A*), or surface labeled and pulsed for 3–5 min followed by an 8-min chase either without (*B*) or with Baf (*C*) followed by acid wash to strip off the surface-bound antibodies and visualize endosomes (as detailed in Fig. 1*A*, step 3). Images were obtained from subapical and medial planes where both Wg and DFz2 are found. The *Insets* (magnified ~2–3×) show the region taken for FRET measurements by donor (A568) dequenching after acceptor photobleaching method. Within the outlined boxes, the acceptor (A647 anti-DFz2) was bleached, and both donor and acceptor intensities, pre- and postbleaching is shown in the panels below. See LUT bar in *E* to compare differences in donor intensities. Endosomes with both Wg and DFz2 (described in Fig. 1 *E* and *F* and step 4 of Fig. 1*A*) were only used for the assay. (*D*) Graph shows FRET efficiencies obtained from outlined images, as in *A–C*, and calculated as described in *SI Materials and Methods*. Note FRET efficiency is much higher in endosomes compared with that at the cell surface ($P < 10^{-12}$), and decreases upon neutralization of the pH of endosomes with Baf ($P < 10^{-10}$). Control used here are punctae labeled with only the donor fluorophore. (*E* and *F*) Confocal images (*E*) of surface-labeled wing discs maintained on ice for 2 h at pH 6.0, and corresponding graph (*F*) shows FRET efficiencies between Wg and DFz2 on surface at pH 6.0 or 7.2. The data indicate that the efficiency is enhanced upon incubation in acidic environment ($P < 10^{-15}$). Data represented is average (±SEM) of FRET efficiencies taken from 60 to 100 structures (endosomes or surface clusters) from four to five discs from two separate experiments. (*G–I*) Confocal images of wing discs depicting the distribution of Wg signal transduction cascade downstream player, Dsh-GFP (expressed under its native promoter), upon incubating wing discs at different pH on ice. *Z* projection of subapical planes is shown in *G* and graphs show the distribution (*H*) and the average intensities from planes enriched in the Dsh-GFP spots (*I*) in response to the incubation at different pH. Significantly more Dsh-GFP is recruited to enriched clusters at lower pH ($P < 10^{-3}$), and their distribution is uniform at pH 6.3 (D, dorsal; V, ventral). All images are background-subtracted and intensities are appropriately scaled for representation. (Scale bars, 10 μm in *A–C* and *E* and 50 μm in *G*.)

spatially graded signaling. Thus, the acidic pH within an endosome plays an important role in promoting Wg–DFz2 interaction to recruit Dsh and sustain Wg signaling within the endosome. Together, these results suggest that Wg and DFz2 interact in a pH-dependent manner within an endosome, and this interaction is necessary for Wg signaling.

Discussion

Multiple pathways of endocytosis ply at the plasma membrane and functional roles for clathrin and dynamin-independent endocytic processes are just beginning to emerge (21). Perturbations of *shibire* and *clathrin* have often been used as tools to evaluate specific roles of endocytosis in either activating signaling [Dpp signaling in wing disc (52)] or attenuating signaling [EGFR signaling in eye discs (53)] during tissue development (8, 54). Here, we have uncovered an in vivo role for the CG endocytic pathway in the regulation of Wg signal transduction in the *Drosophila* wing disc. Our data suggest that a large fraction of Wg is internalized independent of its signaling receptor DFz2 via a Garz, Arf1, and class I PI3K-mediated CG endocytic pathway, and this is necessary for Wg signaling in the wing disc. The fusion of endosomes carrying Wg (apically internalized via the CG pathway) and DFz2 (baso-laterally internalized via the CD pathway), and endosomal acidification, facilitates the interaction of Wg and DFz2, and hence mediates the signaling of Wg (see model in Fig. 8).

A recent study suggests that Wg is internalized from the apical surface via dynamin-dependent endocytosis (55). Here we directly label the endosomes of Wg and DFz2 and track their progression through the endocytic pathway. We find that under conditions wherein dynamin perturbations affects CD cargo (mBSA, TfR) internalization (24, 30), CG-mediated fluid-phase endocytosis is unaffected, Wg continues to be endocytosed, but DFz2 endocytosis is strongly inhibited. On the other hand, Wg endocytosis depends on Garz, Arf1, and class I PI3K, and DFz2 uptake does not. Thus, we conclude that Wg uptake is, to a large extent, dynamin-independent and that both CG and CD endocytosis is used to facilitate Wg–DFz2 interaction within an endosome. To determine the extent of signaling from Wg in endosomes and from the recycled fraction at the baso-lateral surface possibly regulated by Godzilla, as recently proposed (55), more sophisticated assays and minimal signaling systems with fast response times consistent with the time scales of trafficking have to be developed. In addition, because global perturbation of any molecule in the trafficking pathway causes broad-spectrum effects on the kinetics of the entire process, correlating key trafficking molecules with signal transduction remains a challenge.

An important question is how Wg is routed through the CG pathway from the apical surface. The most obvious candidates for a receptor for Wg in the CG pathway are HSPG-containing GPI-anchored proteins or glypicans, which also have a role in Wg signaling (18, 19, 56). In our preliminary experiments, when we measured Wg endocytosis in wing discs that were treated with PI-PLC (phosphatidylinositol-phospholipase C) to remove GPI-anchored proteins, consistent with the loss of receptors/binding sites, the surface levels of Wg are drastically reduced and almost no Wg is endocytosed, whereas DFz2 surface levels and endocytosis are unaffected. This finding argues for a very prominent role of GPI-anchored HSPGs in recruiting Wg to the cell surface, as well as for its endocytosis. Some clathrin and dynamin-independent pathway cargoes drive their own endocytosis when concentrated on the plasma membrane by different binders (57, 58). A similar mechanism can be envisioned for Wg endocytosis via CG pathway, with HSPGs aiding in clustering of Wg at the plasma membrane. However, the identity of the glypican and their role needs further experimentation.

The site of Wnt signaling has been hotly debated. In HeLa cells, Wnts are proposed to form signaling platforms that recruit downstream

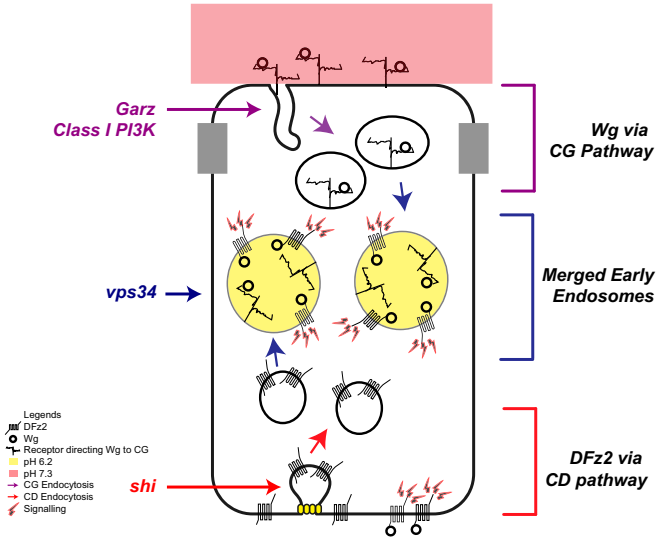

Fig. 8. Model for interaction of Wg and DFz2 in the wing disc Wg and DFz2 are internalized from different surfaces of the polarized wing epithelium via distinct endocytic pathways. Wg interacting with its putative receptor at the apical surface is directed toward the CG pathway, regulated by Arf1, Garz, and class I PI3K, and DFz2 is internalized from the basolateral surface via the CD pathway. The resulting endosomes fuse and the acidification of these endosomes facilitates the interaction of Wg and DFz2. Subsequently, the signal transducers of the Wg–DFz2 assemble at the endosomal membrane and initiate signaling.

players (Dsh, Axin) to the plasma membrane and initiate canonical Wnt signaling (59). However, endocytosis of Wnt3A in L cells (60) and Wg in *Drosophila* wing discs (13, 14, 61) has been shown to be necessary for canonical Wnt signaling as the downstream players are recruited to endosomes (13, 62). In our experiments, Wg interacts productively with DFz2 in the acidified endosome (or when the cell surface is exposed to acidic pH). Hence, it is likely that site of Wg signal is the acidified endosomal membrane. This finding is also consistent with the recruitment of downstream signaling mediators (Dsh and Axin) to these sites of Wg–DFz2 engagement.

Our study, describing the merging of endosomes derived from two distinct surfaces of the wing disc, is reminiscent of trafficking of a number of proteins in other polarized epithelial model systems to a common recycling endosome, which is necessary for their transcytosis. As in the case of a transcytotic cargo, polymeric IgA receptor (63), it is likely that the DFz2 receptor and Wg meet in such a common recycling endosome where signaling may be initiated.

The pleiotropic functions of proteins involved in membrane transport and fission has been noted for many, including clathrin and dynamin (64–66). The functions of the CG pathway have been studied using specific molecular perturbations of Arf1 and its GEF (GBF1/Garz), as well as class I PI3K. It should be noted that although Arf1 and Garz are also important in the early secretory pathway in the formation of COPI-coated vesicles (67), there is mounting evidence of their importance at the plasma membrane. Apart from their role in CG endocytosis (22, 24), Arf1 was shown to be important in generating cortical ventral actin structures (68), and GBF1 was recruited to the leading edge of neutrophils upon activation of PI3Kγ (38). Regulated localization of GBF1 at the Golgi or at the plasma membrane is necessary for its function in either the secretory route or the CG endocytic pathway, respectively. Class I PI3K, which makes PIP3, affects CG endocytosis by regulating the recruitment of Garz to the plasma membrane, and is hence a possible modulator of this switch. PI4,5P2 and PIP3 have been known previously to act as recruiters for various endocytic regulators in CD (69) and bulk endocytosis (70), and here we show a possible mechanism by which PIP3 could affect bulk endocytosis.

Class I PI3K could also serve as a link between two signaling cascades: insulin-mediated growth factor signaling and Wg signaling. Insulin signaling leads to activation of class I PI3K that results in the activation of a cascade of signaling via Akt, which in turn can phosphorylate and deactivate GSK3β and hence affect downstream targets of Wg signaling (46, 71, 72). Given that the effect of class I PI3K on Wg endocytosis is upstream of the role of Akt, the recruitment of Garz is another point of convergence between PI3K and Wg signaling. Such a link between growth, signaling, and endocytic regulation has been previously observed in target of rapamycin signaling where modulation of bulk endocytosis (monitored using dextran) is a mechanism by which cell growth is regulated in fat body cells (73).

Finally, during tissue patterning both cell autonomous and nonautonomous processes are involved in constructing concentration gradients of morphogens. By tuning morphogen–receptor interactions, cells can convert this gradient-based information into differential transcriptional readouts, thus using the same signaling cues for diverse pattern formation (74). The mechanism that we have uncovered coordinates different endocytic pathways to bring together a ligand–receptor pair and facilitate their interaction in the low pH environment of the endosome. Although the existence of different modes of endocytosis have been known (21, 75), this study provides a step toward understanding their interplay in vivo. This could be a general principle, applicable in many contexts where fine-tuning the signal is important.

Materials and Methods

Endocytic assays were conducted on live wing discs preincubated with fluorescently tagged probes and incubated at indicated temperatures for specified times followed by a chase in the absence of the probes, to mark endocytosed Wg and DFz2. FRET studies to study the interaction of Wg and DFz2 at the surface of the epithelium or in endosomes were conducted on discs incubated with fluorescently tagged antibody as indicated. FRET efficiencies were determined using the formula $E = (I_{post} - I_{pre})/I_{post}$, where I_{pre} and I_{post} are the donor intensities, pre- and postbleaching of acceptor from the indicated regions of interest (ROIs). Each assay is described in detail in the figure legends. All reagents, detailed experimental procedures, quantitation, and statistical analysis are provided in *SI Materials and Methods*.

ACKNOWLEDGMENTS. We thank Sanjeev Sharma and Swarna Matre (Raghu Padinjat's laboratory) for extensive help with PI3K reagents; members of the fly community for their generosity in sharing reagents (especially Vivian Budnik, Stefan Luschnig, Xinhua Lin, Hugo Bellen, Raghu Padinjat, Jean Paul Vincent, and Ramanuj Dasgupta); members of the S.M. and Vijay Raghavan laboratories for critically reading the manuscript; and the Central Imaging and Flow cytometry Facility, National Centre for Biological Sciences, where all confocal imaging in the manuscript was done. This work was supported in part by a graduate fellowship from the National Centre for Biological Sciences and Council of Scientific and Industrial Research (to A.H.L. and C.P.), and a JC Bose Fellowship from the Department of Science and Technology, a Margadarshi Fellowship IA/M/15/1/502018 (Wellcome Trust–Department of Biotechnology, India, Alliance), and a Centre of Excellence Grant BT/01/COE/09/01 (Department of Biotechnology), all awarded from the Government of India to S.M.

1. Nusse R, Varmus H (2012) Three decades of Wnts: A personal perspective on how a scientific field developed. *EMBO J* 31(12):2670–2684.
2. Clevers H, Nusse R (2012) Wnt/β-catenin signaling and disease. *Cell* 149(6): 1192–1205.
3. Bhanot P, et al. (1996) A new member of the frizzled family from *Drosophila* functions as a Wingless receptor. *Nature* 382(6588):225–230.
4. Bhanot P, et al. (1999) Frizzled and Dfrizzled-2 function as redundant receptors for Wingless during *Drosophila* embryonic development. *Development* 126(18): 4175–4186.
5. Zecca M, Basler K, Struhl G (1996) Direct and long-range action of a Wingless morphogen gradient. *Cell* 87(5):833–844.
6. Cadigan KM, Fish MP, Rulifson EJ, Nusse R (1998) Wingless repression of *Drosophila* frizzled 2 expression shapes the Wingless morphogen gradient in the wing. *Cell* 93(5): 767–777.
7. Müller P, Rogers KW, Yu SR, Brand M, Schier AF (2013) Morphogen transport. *Development* 140(8):1621–1638.
8. Gonzalez-Gaitan M, Jülicher F (2014) The role of endocytosis during morphogenetic signaling. *Cold Spring Harb Perspect Biol* 6(7):a016881.

9. Franch-Marro X, et al. (2008) Wingless secretion requires endosome-to-Golgi retrieval of Wntless/Evi/Sprinter by the retromer complex. *Nat Cell Biol* 10(2):170–177.
10. Port F, et al. (2008) Wingless secretion promotes and requires retromer-dependent cycling of Wntless. *Nat Cell Biol* 10(2):178–185.
11. Strigini M, Cohen SM (2000) Wingless gradient formation in the *Drosophila* wing. *Curr Biol* 10(6):293–300.
12. Marois E, Mahmoud A, Eaton S (2006) The endocytic pathway and formation of the Wingless morphogen gradient. *Development* 133(2):307–317.
13. Seto ES, Bellen HJ (2006) Internalization is required for proper Wingless signaling in *Drosophila melanogaster*. *J Cell Biol* 173(1):95–106.
14. Rives AF, Rochlin KM, Wehrli M, Schwartz SL, DiNardo S (2006) Endocytic trafficking of Wingless and its receptors, Arrow and DFrizzled-2, in the *Drosophila* wing. *Dev Biol* 293(1):268–283.
15. Alexandre C, Baena-Lopez A, Vincent J-P (2014) Patterning and growth control by membrane-tethered Wingless. *Nature* 505(7482):180–185.
16. Baeg GH, Lin X, Khare N, Baumgartner S, Perrimon N (2001) Heparan sulfate proteoglycans are critical for the organization of the extracellular distribution of Wingless. *Development* 128(1):87–94.
17. Baeg G-H, Selva EM, Goodman RM, Dasgupta R, Perrimon N (2004) The Wingless morphogen gradient is established by the cooperative action of Frizzled and heparan sulfate proteoglycan receptors. *Dev Biol* 276(1):89–100.
18. Tsuda M, et al. (1999) The cell-surface proteoglycan Dally regulates Wingless signalling in *Drosophila*. *Nature* 400(6741):276–280.
19. Yan D, Wu Y, Feng Y, Lin S-C, Lin X (2009) The core protein of glypican Dally-like determines its biphasic activity in wingless morphogen signaling. *Dev Cell* 17(4):470–481.
20. Sabharanjak S, Sharma P, Parton RG, Mayor S (2002) GPI-anchored proteins are delivered to recycling endosomes via a distinct cdc42-regulated, clathrin-independent pinocytic pathway. *Dev Cell* 2(4):411–423.
21. Mayor S, Parton RG, Donaldson JG (2014) Clathrin-independent pathways of endocytosis. *Cold Spring Harb Perspect Biol* 6(6):a016758.
22. Kumari S, Mayor S (2008) ARF1 is directly involved in dynamin-independent endocytosis. *Nat Cell Biol* 10(1):30–41.
23. Chadda R, et al. (2007) Cholesterol-sensitive Cdc42 activation regulates actin polymerization for endocytosis via the GEEC pathway. *Traffic* 8(6):702–717.
24. Gupta GD, et al. (2009) Analysis of endocytic pathways in *Drosophila* cells reveals a conserved role for GBF1 in internalization via GEECs. *PLoS One* 4(8):e6768.
25. Mathew D, et al. (2005) Wingless signaling at synapses is through cleavage and nuclear import of receptor DFrizzled2. *Science* 310(5752):1344–1347.
26. Wu J, Klein TJ, Mlodzik M (2004) Subcellular localization of frizzled receptors, mediated by their cytoplasmic tails, regulates signaling pathway specificity. *PLoS Biol* 2(7):E158.
27. Kalia M, et al. (2006) Arf6-independent GPI-anchored protein-enriched early endosomal compartments fuse with sorting endosomes via a Rab5/phosphatidylinositol-3′-kinase-dependent machinery. *Mol Biol Cell* 17(8):3689–3704.
28. Sriram V, Krishnan KS, Mayor S (2003) Deep-orange and carnation define distinct stages in late endosomal biogenesis in *Drosophila melanogaster*. *J Cell Biol* 161(3):593–607.
29. Gorvel JP, Chavrier P, Zerial M, Gruenberg J (1991) rab5 controls early endosome fusion in vitro. *Cell* 64(5):915–925.
30. Guha A, Sriram V, Krishnan KS, Mayor S (2003) *Shibire* mutations reveal distinct dynamin-independent and -dependent endocytic pathways in primary cultures of *Drosophila* hemocytes. *J Cell Sci* 116(Pt 16):3373–3386.
31. Grigliatti TA, Hall L, Rosenbluth R, Suzuki DT (1973) Temperature-sensitive mutations in *Drosophila melanogaster*. *Mol Gen Genet* 120(2):107–114.
32. Kosaka T, Ikeda K (1983) Possible temperature-dependent blockage of synaptic vesicle recycling induced by a single gene mutation in *Drosophila*. *J Neurobiol* 14(3):207–225.
33. Chen ML, et al. (2002) Unique biochemical and behavioral alterations in *Drosophila shibire*(ts1) mutants imply a conformational state affecting dynamin subcellular distribution and synaptic vesicle cycling. *J Neurobiol* 53(3):319–329.
34. Swetha MG, et al. (2011) Lysosomal membrane protein composition, acidic pH and sterol content are regulated via a light-dependent pathway in metazoan cells. *Traffic* 12(8):1037–1055.
35. Bard F, et al. (2006) Functional genomics reveals genes involved in protein secretion and Golgi organization. *Nature* 439(7076):604–607.
36. Wendler F, et al. (2010) A genome-wide RNA interference screen identifies two novel components of the metazoan secretory pathway. *EMBO J* 29(2):304–314.
37. Armbruster K, Luschnig S (2012) The *Drosophila* Sec7 domain guanine nucleotide exchange factor protein Gartenzwerg localizes at the *cis*-Golgi and is essential for epithelial tube expansion. *J Cell Sci* 125(Pt 5):1318–1328.
38. Mazaki Y, Nishimura Y, Sabe H (2012) GBF1 bears a novel phosphatidylinositol-phosphate binding module, BP3K, to link PI3Kγ activity with Arf1 activation involved in GPCR-mediated neutrophil chemotaxis and superoxide production. *Mol Biol Cell* 23(13):2457–2467.
39. Vlahos CJ, Matter WF, Hui KY, Brown RF (1994) A specific inhibitor of phosphatidylinositol 3-kinase, 2-(4-morpholinyl)-8-phenyl-4H-1-benzopyran-4-one (LY294002). *J Biol Chem* 269(7):5241–5248.
40. McNamara CR, Degterev A (2011) Small-molecule inhibitors of the PI3K signaling network. *Future Med Chem* 3(5):549–565.
41. Neumann CJ, Cohen SM (1997) Long-range action of Wingless organizes the dorsal-ventral axis of the *Drosophila* wing. *Development* 124(4):871–880.
42. DasGupta R, Kaykas A, Moon RT, Perrimon N (2005) Functional genomic analysis of the Wnt-wingless signaling pathway. *Science* 308(5723):826–833.
43. Coghlan MP, et al. (2000) Selective small molecule inhibitors of glycogen synthase kinase-3 modulate glycogen metabolism and gene transcription. *Chem Biol* 7(10):793–803.
44. Stocker H, Hafen E (2000) Genetic control of cell size. *Curr Opin Genet Dev* 10(5):529–535.
45. Fang D, et al. (2007) Phosphorylation of β-catenin by AKT promotes β-catenin transcriptional activity. *J Biol Chem* 282(15):11221–11229.
46. Hu T, Li C (2010) Convergence between Wnt-β-catenin and EGFR signaling in cancer. *Mol Cancer* 9:236.
47. Ye X, Deng Y, Lai Z-C (2012) Akt is negatively regulated by Hippo signaling for growth inhibition in *Drosophila*. *Dev Biol* 369(1):115–123.
48. Gadella TW, Jr, Jovin TM (1995) Oligomerization of epidermal growth factor receptors on A431 cells studied by time-resolved fluorescence imaging microscopy. A stereochemical model for tyrosine kinase receptor activation. *J Cell Biol* 129(6):1543–1558.
49. Yoshimori T, Yamamoto A, Moriyama Y, Futai M, Tashiro Y (1991) Bafilomycin A1, a specific inhibitor of vacuolar-type H(+)-ATPase, inhibits acidification and protein degradation in lysosomes of cultured cells. *J Biol Chem* 266(26):17707–17712.
50. Cruciat C-M, et al. (2010) Requirement of prorenin receptor and vacuolar H+-ATPase-mediated acidification for Wnt signaling. *Science* 327(5964):459–463.
51. Juhász G, et al. (2008) The class III PI(3)K Vps34 promotes autophagy and endocytosis but not TOR signaling in *Drosophila*. *J Cell Biol* 181(4):655–666.
52. Belenkaya TY, et al. (2004) *Drosophila* Dpp morphogen movement is independent of dynamin-mediated endocytosis but regulated by the glypican members of heparan sulfate proteoglycans. *Cell* 119(2):231–244.
53. Legent K, Steinhauer J, Richard M, Treisman JE (2012) A screen for X-linked mutations affecting *Drosophila* photoreceptor differentiation identifies Casein kinase 1α as an essential negative regulator of wingless signaling. *Genetics* 190(2):601–616.
54. Bökel C, Brand M (2014) Endocytosis and signaling during development. *Cold Spring Harb Perspect Biol* 6(3):a017020.
55. Yamazaki Y, et al. (2016) Godzilla-dependent transcytosis promotes Wingless signalling in *Drosophila* wing imaginal discs. *Nat Cell Biol* 18(4):451–457.
56. Lin X, Perrimon N (1999) Dally cooperates with *Drosophila* Frizzled 2 to transduce Wingless signalling. *Nature* 400(6741):281–284.
57. Römer W, et al. (2010) Actin dynamics drive membrane reorganization and scission in clathrin-independent endocytosis. *Cell* 140(4):540–553.
58. Renard H-F, et al. (2015) Endophilin-A2 functions in membrane scission in clathrin-independent endocytosis. *Nature* 517(7535):493–496.
59. Bilic J, et al. (2007) Wnt induces LRP6 signalosomes and promotes dishevelled-dependent LRP6 phosphorylation. *Science* 316(5831):1619–1622.
60. Blitzer JT, Nusse R (2006) A critical role for endocytosis in Wnt signaling. *BMC Cell Biol* 7(1):28.
61. Piddini E, Marshall F, Dubois L, Hirst E, Vincent J-P (2005) Arrow (LRP6) and Frizzled2 cooperate to degrade Wingless in *Drosophila* imaginal discs. *Development* 132(24):5479–5489.
62. Taelman VF, et al. (2010) Wnt signaling requires sequestration of glycogen synthase kinase 3 inside multivesicular endosomes. *Cell* 143(7):1136–1148.
63. Weisz OA, Rodriguez-Boulan E (2009) Apical trafficking in epithelial cells: Signals, clusters and motors. *J Cell Sci* 122(Pt 23):4253–4266.
64. Cao H, Thompson HM, Krueger EW, McNiven MA (2000) Disruption of Golgi structure and function in mammalian cells expressing a mutant dynamin. *J Cell Sci* 113(Pt 11):1993–2002.
65. Kasai K, Shin HW, Shinotsuka C, Murakami K, Nakayama K (1999) Dynamin II is involved in endocytosis but not in the formation of transport vesicles from the trans-Golgi network. *J Biochem* 125(4):780–789.
66. Hirst J, Robinson MS (1998) Clathrin and adaptors. *Biochim Biophys Acta* 1404(1-2):173–193.
67. Donaldson JG, Jackson CL (2011) ARF family G proteins and their regulators: Roles in membrane transport, development and disease. *Nat Rev Mol Cell Biol* 12(6):362–375.
68. Caviston JP, Cohen LA, Donaldson JG (2014) Arf1 and Arf6 promote ventral actin structures formed by acute activation of protein kinase C and Src. *Cytoskeleton (Hoboken)* 71(6):380–394.
69. Jost M, Simpson F, Kavran JM, Lemmon MA, Schmid SL (1998) Phosphatidylinositol-4,5-bisphosphate is required for endocytic coated vesicle formation. *Curr Biol* 8(25):1399–1402.
70. Czech MP (2000) PIP2 and PIP3: Complex roles at the cell surface. *Cell* 100(6):603–606.
71. Fukumoto S, et al. (2001) Akt participation in the Wnt signaling pathway through Dishevelled. *J Biol Chem* 276(20):17479–17483.
72. Anderson EC, Wong MH (2010) Caught in the Akt: Regulation of Wnt signaling in the intestine. *Gastroenterology* 139(3):718–722.
73. Hennig KM, Colombani J, Neufeld TP (2006) TOR coordinates bulk and targeted endocytosis in the *Drosophila melanogaster* fat body to regulate cell growth. *J Cell Biol* 173(6):963–974.
74. Wolpert L (1969) Positional information and the spatial pattern of cellular differentiation. *J Theor Biol* 25(1):1–47.
75. Johannes L, Parton RG, Bassereau P, Mayor S (2015) Building endocytic pits without clathrin. *Nat Rev Mol Cell Biol* 16(5):311–321.